

Crisis bifurcations in plane Poiseuille flow

Stefan Zammert and Bruno Eckhardt

*Fachbereich Physik, Philipps-Universität Marburg, D-35032 Marburg, Germany and
J.M. Burgerscentrum, Delft University of Technology, 2628 CD Delft, The Netherlands*

Direct numerical simulations of transitional plane Poiseuille flow in a mirror-symmetric subspace reveal several interior and exterior crisis bifurcations. They appear in the upper branch that emerges in a saddle-node bifurcation near $\text{Re}_{SN} = 641$ and then undergoes several bifurcations into a chaotic attractor. Near $\text{Re}_{XC} = 785.95$ the attractor collides with the lower-branch state and turns into a chaotic saddle in an exterior crisis, with a characteristic $(\text{Re} - \text{Re}_{XC})^{-\delta}$ variation in lifetimes. For intermediate Reynolds numbers, the attractor undergoes several interior crises, in which new states appear and intermittent behavior can be observed. They contribute to increasing the complexity of the dynamics and to a more dense coverage of state space. The exterior crisis marks the onset of transient turbulence in this subspace of plane Poiseuille flow.

Numerical and experimental studies of pipe and plane Couette flow have demonstrated the significance of exact coherent structures and their bifurcations for the transition to turbulence[1–4]. Typically, these states appear in saddle-node bifurcations and then undergo further bifurcations. Initially, most of their complexity lies in the temporal dynamics, so that they are better characterized as chaotic rather than turbulent. With increasing Reynolds number, more temporal and spatial degrees of freedom are activated, until the complexity of a turbulent flow is established. Many details of this transition scenario have been discussed in plane Couette flow[2] and pipe flow[4, 5]. One contribution of the present study is to demonstrate similar phenomenology for plane Poiseuille flow (PPF). A second one is the demonstration of further phenomena familiar from low-dimensional dynamical systems, such as interior crisis, and their contribution to increasing the complexity of the attractor and of the state space region covered by it.

PPF is the pressure driven flow between two parallel plates and differs from plane Couette flow and pipe flow because of the presence of a linear instability to transverse vortices, the so-called Tollmien-Schlichting modes [6–8]. It occurs at a critical Reynolds number of 5772.22 for a streamwise wavenumber α of 1.02056, as determined by Orszag [9]. The bifurcation is subcritical, and reaches down to about $\text{Re} \approx 2700$ [10, 11] (for different wavelength). However, several experiments and numerical simulations show that turbulence occurs already at Reynolds numbers around 1000 [12–14], and hence well below the onset of Tollmien-Schlichting modes. Thus, the linear instability cannot explain the observed turbulence at low Reynolds numbers and the situation becomes analogous to that in plane Couette and pipe flow.

In order to determine the relevant saddle-node bifurcation in PPF we use the method of edge tracking, as described in [15], see also [16]. The method traces the time-evolution of initial conditions and uses bisection between an initial condition that returns to the laminar profile and one that becomes turbulent to approximate one on the laminar-turbulent interface. In most cases the state evolves towards a simple attractor, such as a fixed point or a simple periodic orbit. It is then possible to continue

the edge state in Reynolds number around the saddle-node bifurcation and to identify the upper branch solution. In recent work for plane Couette[2] and pipe flow[4] it was shown that the upper branch of the edge state undergoes various bifurcations resulting in a chaotic attractor. A boundary or exterior crisis ultimately destroys this stable attractor and creates the observed transient turbulence with its characteristic exponentially distributed lifetimes. The observed phenomenology is similar to what has been described and discussed in the context of chaotic dynamical systems [17, 18].

We will here show that this scenario is also present in plane Poiseuille flow and that another type of crisis bifurcation, the interior crisis, provides a mechanism by which the part of state space occupied by the chaotic attractor can increase. Furthermore, we will discuss mechanisms for the observed increase of lifetimes of chaotic transients [19].

For our numerical simulations we use the *Channelflow*-code [20]. The Reynolds number $\text{Re} = U_0 d / \nu$ for the system is based on half the distance between the plates d , the maximum velocity of the laminar profile U_0 and the kinematic viscosity ν . We take a coordinate system in which x points in the streamwise, z in the spanwise and y in the wall-normal direction. With the above choices for the dimensionless units the laminar profile becomes $\vec{u}_l(y) = (U(y), 0, 0)$ with $U(y) = 1 - y^2$. The total flow field \vec{u}_t can be written as the sum of the laminar profile and a fluctuating component, $\vec{u}_t = \vec{u}_l + \vec{u}$. All simulations in the paper are performed for constant mass flux. The calculations are restricted to a computational domain of length 2π , width π (and height 2) in a subspace that is symmetric to reflections at the midplane and to spanwise reflections at the plane defined by $z = 0$:

$$s_y : [u, v, w](x, y, z) = [u, -v, w](x, -y, z) \quad (1)$$

$$s_z : [u, v, w](x, y, z) = [u, v, -w](x, y, -z) \quad (2)$$

The numerical resolution is $N_x \times N_y \times N_z = 48 \times 65 \times 48$ modes.

Using the technique of edge tracking it is possible to identify the edge state [15, 21] of this system. A trajectory on the laminar-turbulent boundary quickly reaches

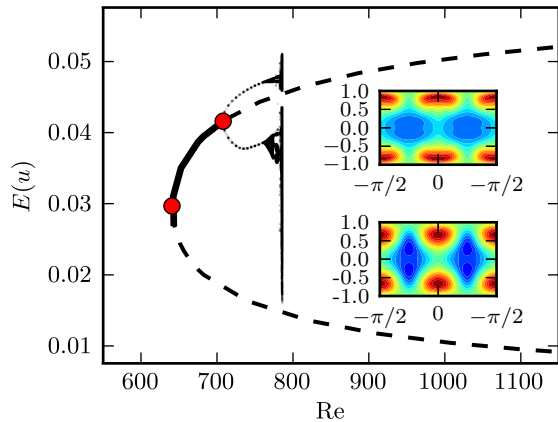


FIG. 1. Bifurcation diagram for the travelling wave TW_{Eyz} . Solid lines indicate a stable state, dashed lines an unstable state. Chaotic and periodic states are indicated by clouds of points obtained by plotting minima and maxima of their energy densities in the course of time. The red dots indicate the bifurcation point of TW_{Eyz} and PO_{yz} , respectively. The insets show the average streamwise velocity in the spanwise-wallnormal plane for the lower and the upper branch of TW_{Eyz} at $Re = 830$. The colors indicate low (blue) and high (red) velocity regions.

a states of constant energy. Since a stationary state is ruled out on account of the non-zero mean flow, the attractor in the laminar-turbulent boundary is a travelling wave. Indeed, a Newton search [22] for a relative equilibrium converges to a traveling wave, henceforth referred to as TW_{Eyz} . The form of the state is indicated in the inset in Fig. 1. The travelling wave has the same symmetries as the mirror-symmetric travelling wave previously described by Nagata and Deguchi [23] and Gibson and Brandt [24].

We use a continuation method (see e.g. [25]) to follow the solutions in Reynolds number around the saddle-node bifurcation at $Re_{SN} = 641$. A stability analysis of the travelling wave shows that in the symmetry subspace the lower branch has one unstable eigenvalue and the upper branch is stable for $641 < Re < 707$.

At $Re = 707$ the upper branch undergoes a Hopf bifurcation that creates a stable relative periodic orbit PO_{yz} . This orbit undergoes a Neimark-Sacker bifurcation at $Re = 761.5$ that creates a stable torus. In further bifurcations a chaotic attractor is generated. By plotting minima and maxima of the energy

$$E(\vec{u}) = \frac{1}{2L_x L_z} \int_0^{L_z} \int_{-1}^1 \int_0^{L_x} \vec{u}^2 dx dy dz \quad (3)$$

of a trajectory on the attractor we are able to map out the bifurcation diagrams also in chaotic regions, as shown in Fig. 1.

The magnification of the chaotic attractor in Fig. 2 highlights the two phenomena we want to focus on here: Slightly above $Re = 785$ (blue line) the size of

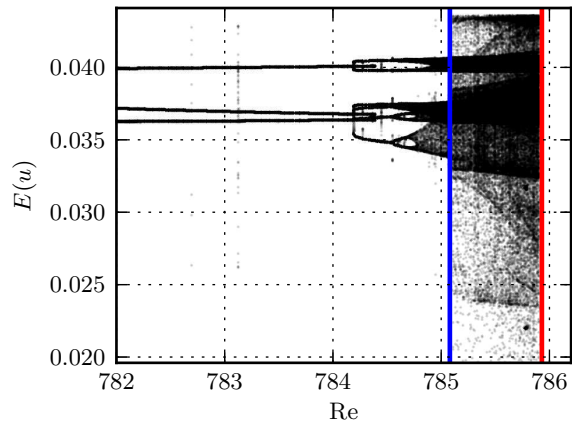


FIG. 2. Magnification of the attractor in Fig. 1 in order to highlight the interior crisis (blue line) and the exterior crisis (red line). The states are visualized by plotting minima of $E(u)$ along trajectories.

the attractor expands and covers a larger fraction of the interval, and slightly below $Re = 786$ (red line) it disappears. Both changes are connected with crisis bifurcations [17, 18], an interior crisis in the first case, and an exterior crisis in the second case.

Slightly above $Re = 785$ the points on the attractor suddenly spread over a wider region, covering the area in state space with an energy E between 0.023 and 0.044. However, these parts of the state space are only visited occasionally, so that the points are less dense than in other parts. The reason for the sudden enlargement is a so-called interior crisis bifurcation [26, 27], where a new state appears and new links to the attractor form. The appearance of the new states can be seen in the time series in Fig. 3. Just before the crisis, the range of the trajectories is limited to the interval $[0.033, \dots, 0.042]$. Slightly above the crisis, excursions to lower values occur, with their number increasing with Re .

The type of transition can be determined from the distribution of times spent in the different regions. The state space region covered by the attractor before the crisis, referred to as phase A , contains trajectories that never drop below a threshold in energy, here taken to be $E_t = 0.031$. If the trajectory drops below E_t , trajectories enter a different phase B , occupying a different region in state space. An indicator for phase B are the repeated excursions to values below E_t . Accordingly, if no excursions are noted for more 250 time units, we conclude that the system has returned to phase A . With this prescription one can determine the distribution of times in phase A as shown in Fig. 4a. The plot contains data from trajectories with a total length of $5 \cdot 10^6$ time units. The data are shown semi-logarithmically, so that the times are compatible with an exponential distribution, as expected for an interior crisis [28, 29]. We then fit an exponential decay to the distribution to obtain

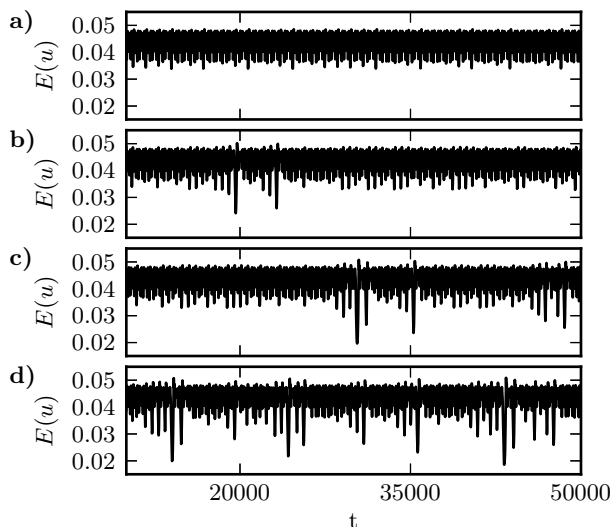


FIG. 3. Energy traces $E(t)$ for trajectories near the interior crisis. (a) $Re = 785.0$, slightly below the crisis. (b), (c), and (d) are for $Re = 785.46$, 785.75 , and 785.9 , respectively, above the crisis. They show the characteristic intermittent bursts.

the characteristic trapping times τ_A in phase A and plot them versus Reynolds number in Fig. 4b. Approaching the crisis point from above, the time in phase A diverges since B is never visited. According to [18, 28] the characteristic time varies as

$$\tau_A \propto (Re - Re_{IC})^{-\gamma} \quad (4)$$

with an exponent γ . In the present case we obtain a good fit to the data with $Re_{IC} = 785.097$ and $\gamma = 0.786$. This exponent can be shown to be $\gamma = 0.5$ for 1-dimensional maps [30], but in higher dimensional system larger exponents have also been observed [17, 18, 31].

Typical turbulent trajectories show an enormous temporal and spatial complexity that is difficult to create in a sequence of simple Neimark-Sacker or period-doubling bifurcations. As is evident from Fig. 3 the dynamics of the system is rather regular (but not periodic!) before the interior crises and becomes increasingly more complicated (both in the range covered and in the complexity of the time-signal) as the Reynolds number increases. Thus, the interior crisis bifurcation increases the complexity of the chaotic trajectories more dramatically than other local bifurcations and are an important contribution towards more turbulent time evolutions.

The second phenomenon we want to address here is the change in the dynamics near $Re = 786.5$, where the chaotic attractor suddenly disappears. Here, the attractor collides with the lower-branch state and turns into a chaotic saddle in a boundary or exterior crisis bifurcation [26]. It is a generic property of a chaotic saddle that the survival probabilities are exponentially distributed. To quantify this defining property of the boundary crisis, the survival probabilities for $Re > Re_{XC}$ are calculated using the methods described by [32]. The survival prob-

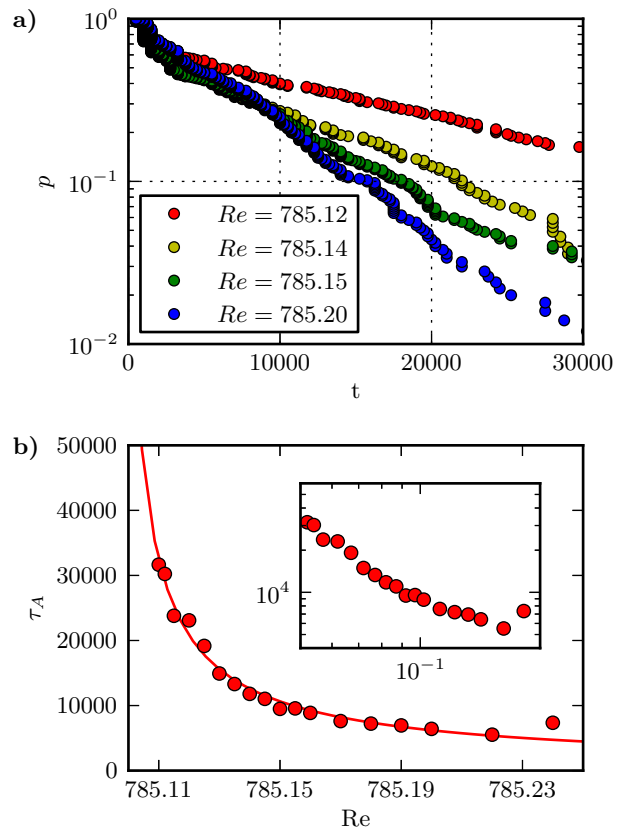


FIG. 4. Intermittency near the interior crisis. (a) Probability to stay t time units in the pre-crisis phase A. The times are exponentially distributed and the characteristic timescale τ_A increases with decreasing distance to Re_{IC} . (b) Variation of characteristic times with Reynolds number. The continuous line shows an algebraic fit to equation (4) with $\gamma = 0.786$. The inset shows the same data on a doubly logarithmic scale.

abilities are clearly exponentially distributed with characteristic lifetimes that depend on the Reynolds number, as shown in Fig. 5. As in the case of the interior crisis they diverge as

$$\tau \propto (Re - Re_{XC})^{-\delta} \quad (5)$$

at the Reynolds number Re_{XC} of the crisis bifurcation. Best fits to the data are obtained for $\delta = 1.05$ and $Re_{XC} = 786.48$, as expected for an exterior crisis.

A dense sampling of initial conditions in the state space of the system combined with a fine scan of Reynolds numbers in the range between $Re = 778.3$ and $Re = 780.6$ reveals a small attractor A_{1a} inside of A_1 . This attractor disappears at $Re = 780.6$ in another boundary crisis bifurcation and above this Reynolds number initial conditions exist that transiently visit the saddle created by the boundary crisis of the attractor A_{1b} before suddenly settling down on A_1 . An example for such a trajectory is shown in Fig. 6. Furthermore, no initial conditions can be found that transiently visit the saddle before becoming laminar. This behavior is strong evidence that

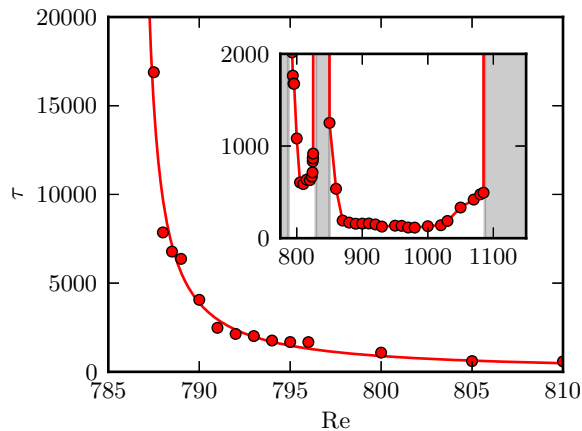


FIG. 5. Characteristic lifetimes τ vs. Reynolds number above the boundary crisis. The continuous line is an algebraic fit to equation (4) with $\delta = 1.05$. The inset shows τ for a larger range in Re. The points are connected to guide the eye only. Regions where a stable attractor exists are shaded grey; the lifetime τ is infinite in these regions.

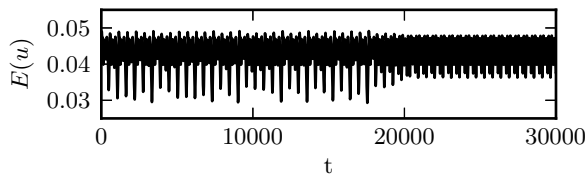


FIG. 6. Transition between saddle A_{1b} and attractor A_1 in the energy trace of a trajectory at $Re = 780.7$. The trajectory stays on the chaotic saddle A_{1b} for about 18000 time units before it suddenly switches to the stable attractor A_1 .

A_{1a} lies completely inside of the basin of A_1 . The presence of the chaotic saddle created in the boundary crisis of A_{1a} should lead to a second slope in the lifetime distribution as also seen in [33]. But since the basin of A_{1a} is very small compared to A_1 this slope does not

influence the characteristic lifetimes in Fig. 5. The lifetimes for a larger range in Re are shown in the inset of Fig. 5. Following the boundary crisis the lifetimes of the chaotic transients first decrease, then start to increase again around $Re \approx 815$, and diverge at $Re = 828$, where a second stable attractor (A_2) appears. At slightly higher Re another attractor (A_3) appears so that including the laminar state for a small range in Re the system has three attracting states. A_2 and A_3 disappear in a boundary crises at $Re = 837.5$ and $Re = 841.8$, respectively. After the boundary crisis of A_3 the lifetimes drop to even lower values than before the appearance of A_2 . They decrease until $Re = 930$, where a lifetime of 126 is reached. Afterwards lifetimes increase again and eventually diverge at $Re = 1087$, where another attractor A_4 appears. The attractors A_2 - A_4 appear in regions of the state space occupied by the large saddle created in the boundary crisis of A_1 , as was checked using slices of the state space as in [33].

The crisis bifurcations analyzed here for PPF underline and extend previous observations on Couette flow[33] and also pipe flow [34] in that they provide further examples of smaller chaotic saddles inside larger outer saddles and of bifurcations that contribute to an increase of the characteristic lifetimes and eventually to a more complex temporal dynamics. Moreover, the interior crises contribute to a more dense coverage of the state space of the system by the dynamics. Thereby, they pave the way for the transition to a chaotic saddle when the attractor collides with the saddle from the original saddle-node bifurcation. The connection to the phenomenology of low-dimensional dynamical systems and the appearance in a number of canonical flows suggests that this transition scenario is typical for the transition in shear flows.

We thank John Gibson for providing *channelflow* and the participants and organizers of the Euromech Colloquium EC565 “Subcritical transition to turbulence” for fruitful discussions. This work was supported by the Deutsche Forschungsgemeinschaft within FOR 1182.

-
- [1] B. Hof, C. W. H. van Doorne, J. Westerweel, F. T. M. Nieuwstadt, H. Faisst, B. Eckhardt, H. Wedin, R. R. Kerswell, and F. Waleffe, *Science* **305**, 1594 (2004).
 - [2] T. Kreilos and B. Eckhardt, *Chaos* **22**, 047505 (2012).
 - [3] G. Kawahara, M. Uhlmann, and L. van Veen, *Annu. Rev. Fluid Mech.* **44**, 203 (2012).
 - [4] M. Avila, F. Mellibovsky, N. Roland, and B. Hof, *Phys. Rev. Lett.* **110**, 224502 (2013).
 - [5] F. Mellibovsky and B. Eckhardt, *J. Fluid Mech.* **709**, 149 (2012).
 - [6] W. Heisenberg, *Ann. Phys.* **74** (1924).
 - [7] C. Lin, *Quart. Appl. Math.* **3**, 218 (1945).
 - [8] L. Thomas, *Phys. Rev.* **91**, 780 (1953).
 - [9] S. A. Orszag, *J. Fluid Mech.* **50**, 689 (1971).
 - [10] J.-P. Zahn, J. Toomre, E. Spiegel, and D. Gough, *J. Fluid Mech.* **64**, 319 (1974).
 - [11] I. Soibelman and D. I. Meiron, *J. Fluid Mech.* **229**, 389 (1991).
 - [12] D. R. Carlson, S. E. Widnall, and M. F. Peeters, *J. Fluid Mech.* **121**, 487 (1982).
 - [13] G. Lemoult, J.-L. Aider, and J. E. Wesfreid, *Phys. Rev. E* **85**, 1 (2012).
 - [14] L. S. Tuckerman, T. Kreilos, H. Schrobdsdorf, T. M. Schneider, and J. F. Gibson, *Phys. Fluids* **26**, 114103 (2014).
 - [15] J. Skufca, J. A. Yorke, and B. Eckhardt, *Phys. Rev. Lett.* **96**, 174101 (2006).
 - [16] S. Toh and T. Itano, *J. Fluid Mech.* **481**, 67 (2003).
 - [17] T. Tél and Y.-C. Lai, *Phys. Rep.* **460**, 245 (2008).
 - [18] Y.-C. Lai and T. Tél, *Transient Chaos - Complex Dynamics on Finite Time Scales* (Springer New York, 2011).
 - [19] B. Hof, J. Westerweel, T. M. Schneider, and B. Eck-

- hardt, *Nature* **443**, 59 (2006).
- [20] J. F. Gibson, *Channelflow: A spectral Navier-Stokes simulator in C++*, Tech. Rep. (U. New Hampshire, 2012).
- [21] T. M. Schneider, J. F. Gibson, M. Lagha, F. De Lillo, and B. Eckhardt, *Phys. Rev. E* **78**, 037301 (2008).
- [22] D. Viswanath, *J. Fluid Mech.* **580**, 339 (2007).
- [23] M. Nagata and K. Deguchi, *J. Fluid Mech* **735**, R4 (2013).
- [24] J. F. Gibson and E. Brand, *J. Fluid Mech.* **745**, 25 (2014).
- [25] H. Dijkstra, F. W. Wubs, A. K. Cliffe, E. Doedel, I. F. Dragomirescu, B. Eckhardt, A. Y. Gelfgat, A. L. Hazel, V. Lucarini, A. G. Salinger, E. T. Phipps, J. Sanchez-Umbria, H. Schuttelaars, L. S. Tuckerman, and U. Thiele, *Commun. Comput. Phys.* **15**, 1 (2014).
- [26] C. Grebogi, E. Ott, and J. A. Yorke, *Phys. Rev. Lett.* **48**, 1507 (1982).
- [27] C. Grebogi, E. Ott, and J. A. Yorke, *Phys. D Nonlinear Phenom.* **7**, 181 (1983).
- [28] C. Grebogi, E. Ott, F. Romeiras, and J. A. Yorke, *Phys. Rev. A* **36** (1987).
- [29] P. R. Muñoz, J. J. Barroso, A. C.-L. Chian, and E. L. Rempel, *Chaos* **22**, 033120 (2012).
- [30] C. Grebogi, E. Ott, and J. A. Yorke, *Phys. Rev. Lett.* **57** (1986).
- [31] W. L. Ditto, S. Raueo, R. Cawley, C. Grebogi, G.-H. Hsu, E. Kostelich, E. Ott, H. T. Savage, R. Segnan, M. L. Spano, and J. A. Yorke, *Phys. Rev. Lett.* **63**, 923 (1989).
- [32] M. Avila, A. P. Willis, and B. Hof, *J. Fluid Mech.* **646**, 127 (2010).
- [33] T. Kreilos, B. Eckhardt, and T. M. Schneider, *Phys. Rev. Lett.* **112**, 044503 (2014).
- [34] S. Altmeyer, A. Willis, and B. Hof, (2015), [arXiv:1501.0198](https://arxiv.org/abs/1501.0198).